Room-Temperature Spin-Orbit Torque Switching Induced by a Topological Insulator

Jiahao Han,[1] A. Richardella,[2] Saima A. Siddiqui,[1] Joseph Finley,[1] N. Samarth,[2] and Luqiao Liu[1,*]
[1]*Massachusetts Institute of Technology, Cambridge, Massachusetts 02139, USA*
[2]*The Pennsylvania State University, University Park, Pennsylvania 16802, USA*

(Received 25 May 2017; revised manuscript received 28 June 2017; published 18 August 2017)

The strongly spin-momentum coupled electronic states in topological insulators (TI) have been extensively pursued to realize efficient magnetic switching. However, previous studies show a large discrepancy of the charge-spin conversion efficiency. Moreover, current-induced magnetic switching with TI can only be observed at cryogenic temperatures. We report spin-orbit torque switching in a TI-ferrimagnet heterostructure with perpendicular magnetic anisotropy at room temperature. The obtained effective spin Hall angle of TI is substantially larger than the previously studied heavy metals. Our results demonstrate robust charge-spin conversion in TI and provide a direct avenue towards applicable TI-based spintronic devices.

DOI: 10.1103/PhysRevLett.119.077702

Spin-orbit coupling has been extensively studied for the conversion between charge current and spin current [1]. When coupled with a neighboring ferromagnet (FM), nonequilibrium spins induced by the spin-orbit coupling can exert torques onto magnetic moments [Fig. 1(a)], which remarkably manipulates the magnetic dynamics [2–4] and even switches the magnetization [5–7]. This current-induced switching is expected to lead to logic and memory device applications with high-energy efficiency [1]. Topological insulators (TI) are a class of materials with spin-orbit coupling that is strong enough to invert the band structure and leads to complete spin-momentum locking in the surface states [8–11]. Recently, it was shown that by utilizing the current-induced spin-orbit torque (SOT) from TI [12], one could switch the moments in magnetically doped TI heterostructures [13–15]. However, restricted by the low Curie temperature of the employed FM materials, the switching has only been realized at a few Kelvin. Room temperature SOT switching, which lies at the heart of applicative interests, remains to be demonstrated. On the other hand, several different techniques (including spin pumping [16–18], spin torque ferromagnetic resonance [11,12,19], second harmonic magnetometry [13,14], nonlocal spin valve or tunnel junction measurements [10,20–23], and the spin Seebeck effect [24]) have been applied to extract the figure of merit for charge-spin conversion, the effective spin-Hall angle α_{SH}. The obtained results vary by orders of magnitude, which obscures the fundamental understanding of the spin transport mechanism. Moreover, very controversial temperature dependencies of α_{SH} have been reported in different measurements. One question that naturally arises is whether TI can provide spin-orbit coupling that is robust enough for room temperature applications. Therefore, a direct, definitive experimental evidence to illustrate the SOT switching efficiency of TI at room temperature is highly desirable. In this work, by integrating prototypical TI with a ferrimagnet with perpendicular magnetic anisotropy (PMA), we observe current-induced magnetic switching at room temperature, which provides a direct avenue towards applicable TI-based spintronic devices.

A major difficulty in realizing TI-based SOT switching at room temperature is the growth of FM layers with

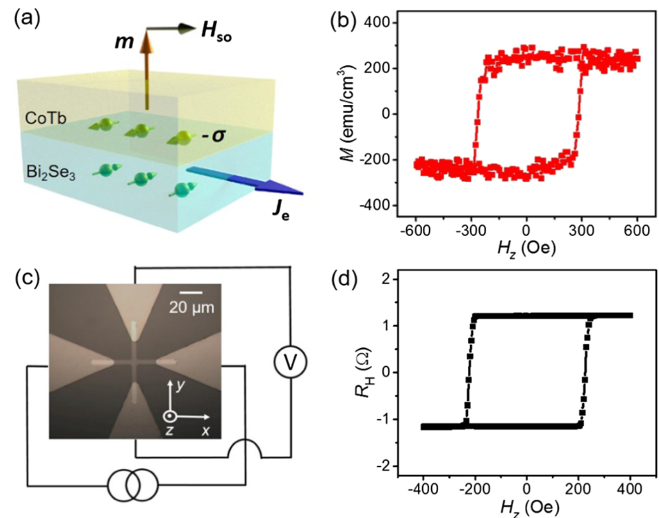

FIG. 1. Structure and magnetic properties of the Bi_2Se_3/CoTb sample. (a) Schematic of SOT in Bi_2Se_3/CoTb heterostructure. The charge current ($\boldsymbol{j}_e$) generates spin accumulation ($-\boldsymbol{\sigma}$) which is perpendicular to the current direction at the interface, and exerts a SOT on the magnetic moments ($\boldsymbol{m}$). The SOT is proportional to $\boldsymbol{m}\times(\boldsymbol{\sigma}\times\boldsymbol{m})$ and can be described by an effective field $\boldsymbol{H}_{SO}$, which is proportional to $\boldsymbol{\sigma}\times\boldsymbol{m}$. (b) Hysteresis loop of the out-of-plane magnetization measured by vibrating sample magnetometry (VSM). (c) Image of the Hall device with an illustration of the electrical measurement setup. The current is applied along the x axis and the Hall voltage is detected in the y direction. The width of the Hall bar is ~4 μm. (d) Anomalous Hall resistance vs out-of-plane magnetic field.

 © 2017 American Physical Society

appropriate magnetic anisotropy neighboring with TI. It is known that the FM layers with PMA can be used for fabricating SOT switching devices with simple device architecture and good thermal stability [5,6]. However, the magnetic anisotropy of the commonly used FM materials such as Co and CoFeB strongly relies on interfacial conditions, which usually favors an in-plane orientation when grown on TI. Comparatively, transition metal–rare earth ferrimagnetic alloys (e.g., Co_xTb_{1-x}) are more promising owing to their robust bulk PMA [25,26]. In CoTb alloys, the sublattices of the Co and Tb elements are antiferromagnetically coupled. The magnetic properties such as the anisotropy energy coefficient and magnetization can be tuned within a wide range of values through chemical composition engineering. In our work, GaAs substrate/Bi_2Se_3 (7.4 nm)/CoTb (4.6 nm)/SiN_x (3 nm) multilayer stacks are deposited through a combination of molecular beam epitaxy [27,28] and magnetron sputtering (see details in Ref. [23]), followed by an insulating SiN_x layer (3 nm) to avoid oxidation. The atomic ratio of the Tb element in CoTb alloy (0.23) and the film thickness (4.6 nm) are chosen to get optimal PMA on the TI material Bi_2Se_3 [Fig. 1(b)]. The resistivities of the Bi_2Se_3 and CoTb layers are determined to be 1060 and 97 $\mu\Omega$ cm using four-point measurements, which is consistent with the measured total resistance of Bi_2Se_3/CoTb/SiN_x multilayer samples. The films are then patterned to Hall bar structures for transport measurements [Fig. 1(c)]. The anomalous Hall resistance (R_H) as a function of applied out-of-plane magnetic field (H_z) is plotted in Fig. 1(d). Thanks to the successful development of the PMA layer with high Curie temperature on top of Bi_2Se_3, for the first time we can observe efficient SOT switching induced by TI at room temperature.

Current-induced switching is measured by sweeping a dc current, while a bias magnetic field (H_x) of 1000 Oe is applied along the current direction to achieve deterministic switching polarities. As plotted in Fig. 2(a), the current switches the magnetization of the CoTb layer between up and down directions, corresponding to the Hall resistance of $\pm 0.6\ \Omega$. The curve changes its polarity when the bias field is inversed [Fig. 2(b)], which is a typical characteristic of the SOT switching of PMA films [6]. The total resistance change (1.2 Ω) is comparable with the $R_H - H_z$ curve under the same in-plane bias field (1.4 Ω [28]), which demonstrates an almost complete magnetization switching with current. The difference of resistance change between current-induced switching and field switching can be explained by the current spreading at the Hall cross [28]. The critical current density in Bi_2Se_3 for switching ($2.8 \times 10^6\ \mathrm{A/cm^2}$, calculated using a parallel circuit model with the resistivity values) is much smaller than the typical values obtained in heavy metal-FM structures with much thinner FM layers [usually in the magnitude of $10^7\ \mathrm{A/cm^2}$, see Refs. [11–13] and Figs. 4(a) and 4(b)], suggesting the high SOT efficiency in Bi_2Se_3.

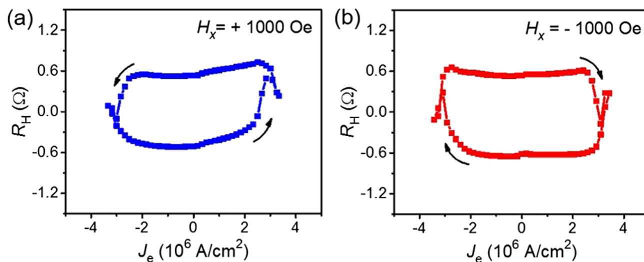

FIG. 2. Room temperature SOT switching in Bi_2Se_3/CoTb. Hall resistance is measured when sweeping a dc current under a bias field of 1000 Oe along (a) the positive and (b) negative x axis. j_e is the average current density inside the Bi_2Se_3 layer.

We now turn to the quantitative calibration of the SOT efficiency in Bi_2Se_3/CoTb heterostructures. When a bias field is applied along the current direction, the dampinglike term of SOT, which is most relevant to the magnetization switching [6], exerts an out-of-plane effective field inside the Néel type domain walls. This effective field is reflected by a horizontal shift in the $R_H - H_z$ hysteresis curve [3,32]. As shown in Fig. 3(a), under a bias field of $H_x = +800$ Oe, the center of the $R_H - H_z$ curves shifts from zero to the positive (negative) side in the presence of a positive

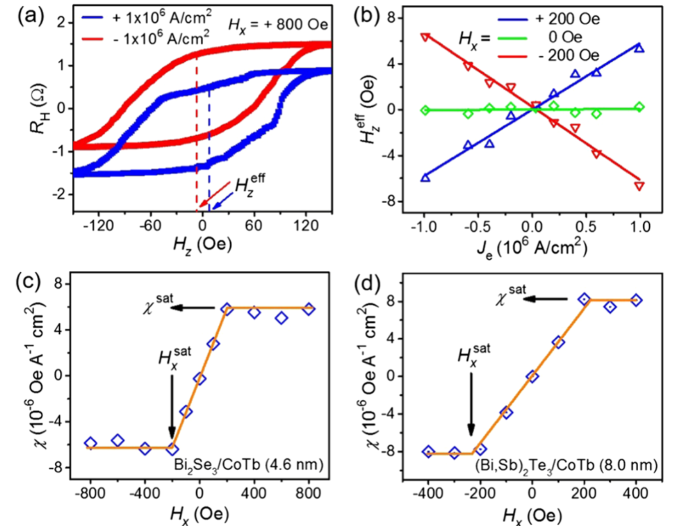

FIG. 3. Calibration of the SOT efficiency. (a) Hall resistance vs applied perpendicular field under positive and negative dc currents with the density of $1.0 \times 10^6\ \mathrm{A/cm^2}$ through Bi_2Se_3 and a bias field $H_x = +800$ Oe. The center shift corresponds to the SOT-induced effective field (H_z^{eff}). (b) H_z^{eff} as a function of applied current under bias fields $H_x = 0, \pm 200$ Oe. (c) SOT efficiency χ vs H_x. χ saturates at the field H_x^{sat}. The data shown in (a) to (c) are measured in the Bi_2Se_3/CoTb sample. (d) SOT efficiency χ vs H_x in the $(Bi,Sb)_2Te_3$/CoTb sample. Note that the magnetization and film thickness of CoTb layers in (c) and (d) differ from each other, which is taken into account during our calculation of α_{SH}.

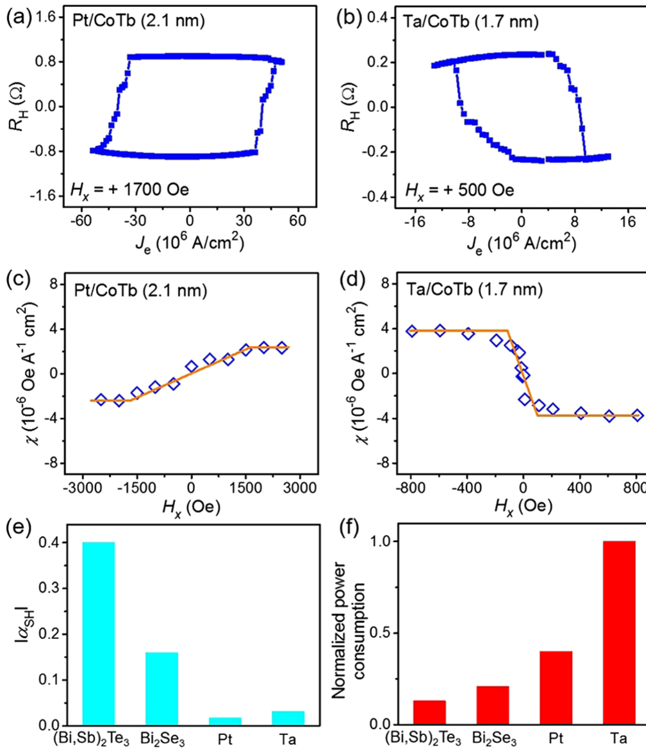

FIG. 4. Comparative measurements of CoTb grown on different spin-orbit materials. (a) and (b) Current-induced switching in Pt/CoTb and Ta/CoTb samples under positive bias fields. (c) and (d) SOT efficiency χ vs bias field H_x in Pt/CoTb and Ta/CoTb samples. Note that compared with the Bi_2Se_3/CoTb sample, CoTb layers with reduced thickness have been used for Pt and Ta samples, to allow for measurable current-induced switching. (e) Absolute values of the effective spin Hall angles of $(Bi,Sb)_2Te_3$, Bi_2Se_3, Pt, and Ta measured by our experiments. (f) Normalized power consumption (with Ta set to be unity) for switching FM electrodes in unit magnetic volume using $(Bi,Sb)_2Te_3$, Bi_2Se_3, Pt, and Ta.

(negative) current. We measure the $R_H - H_z$ hysteresis loops under a series of applied current and H_x, and plot the center of the hysteresis loops (H_z^{eff}) as a function of the current density (j_e) [Fig. 3(b)]. The slope defined as $\chi \equiv H_z^{\mathrm{eff}}/j_e$ represents the dampinglike SOT efficiency, the sign of which depends on the direction of H_x.

The dependence of the SOT efficiency on the bias field is summarized in Fig. 3(c). χ grows linearly in magnitude for small H_x, and reaches saturation (χ^{sat}) when H_x is larger than 200 Oe. The evolution of χ as a function of H_x can be explained by the chirality change of the domain walls in the CoTb layer. The Dzyaloshinskii-Moriya interaction (DMI) can appear either at the Bi_2Se_3/CoTb interface or in the bulk of the CoTb alloy, leading to the formation of the Néel domain walls with a certain chirality. As the bias field increases to overcome the DMI effective field (H_{DMI}), the domain walls change their chirality and start to move in directions that facilitate magnetic switching [3,26,32]. In this scenario, χ^{sat} represents the intrinsic SOT efficiency and the saturating bias field ($H_x^{\mathrm{sat}} \approx 200$ Oe) can serve as an estimation of H_{DMI} and the DMI energy [28].

The effective spin Hall angle (α_{SH}, defined as the ratio between the generated spin current density $(2e/\hbar)j_s$ and the average charge current density in TI j_e) of the Bi_2Se_3/CoTb heterostructure is calculated using [32]

$$\chi^{\mathrm{sat}} = \frac{\pi}{2}\frac{\alpha_{\mathrm{SH}}\hbar}{2e\mu_0 M_s t}, \quad (1)$$

where $\hbar$ is Planck's constant, e is the electron charge, μ_0 is the vacuum permeability, $M_s = 280\ \mathrm{emu/cm^3}$ is the saturated magnetization, and $t = 4.6$ nm is the thickness of the CoTb layer. With the obtained $\chi^{\mathrm{sat}} = 6.1 \times 10^{-6}\ \mathrm{Oe\,A^{-1}\,cm^2}$ in Fig. 3(c), the effective spin Hall angle is determined to be 0.16 ± 0.02. Noticeably, previously reported spin Hall angle of TI varies from 0.01 over 400 [11–23]. The discrepancies may be ascribed to different film qualities and the data fitting process, as well as possible involvement of the magnon scattering mechanism [15]. Compared with the indirect measurements, the method we use is straightforward and more relevant to the real application scenario, where the charge-spin conversion efficiency is directly quantified in the magnetic switching configurations. Besides the absolute values, very different trends have also been observed in the temperature dependence of the charge-spin conversion efficiency previously. While some experiments suggest the immunity of TI to temperature increase [12,18], many others indicate a very quick decay of the efficiency when the temperature is raised above the liquid helium temperature [10,16,19,20], which dims the prospect of TI for applicable switching devices. Our quantification of α_{SH} at room temperature, together with the results in Fig. 2, demonstrate the feasibility of room temperature applications.

It remains a controversial issue whether the surface or bulk states make the dominant contributions to the final SOT in TI [16–19]. This issue becomes most significant for Bi_2Se_3, where very conductive bulk states exist at the Fermi surface [11,12]. To gain further insights on this topic, we employ $(Bi,Sb)_2Te_3$, a more insulating TI, to reduce the bulk effects. According to previous electronic structure [33,34] and transport measurements [17,23], $(Bi,Sb)_2Te_3$ has fewer bulk conductance channels. This is consistent with the resistivity of our $(Bi,Sb)_2Te_3$ layer (4020 $\mu\Omega$ cm), almost 4 times larger than Bi_2Se_3. A CoTb layer (8.0 nm, $M_s = 300\ \mathrm{emu/cm^3}$) with PMA is grown on $(Bi,Sb)_2Te_3$ (8.0 nm) [28]. The SOT efficiency vs in-plane bias field is measured [Fig. 3(d)] using the same method as the Bi_2Se_3 sample. The effective spin Hall angle of $(Bi,Sb)_2Te_3$ is calculated to be 0.40 ± 0.04 according to Eq. (1), which is 2.5 times larger than that of Bi_2Se_3. The fact that TI with reduced bulk conductance leads to a higher spin Hall angle suggests that the topological surface states make significant contributions to the efficient SOT.

To make a direct comparison on the SOT efficiencies between TI and other widely studied heavy metals, we fabricate additional control samples with $Pt/CoTb/SiN_x$ and $Ta/CoTb/SiN_x$ stacks. The resistivities of Pt and Ta are determined to be 23 and 193 $\mu\Omega$ cm. We first try to use CoTb films with the same thickness as the Bi_2Se_3 sample; however, because of the reduced SOT efficiency in these metals, no current-induced switching can be detected. Alternatively, we grow thinner CoTb films (~2 nm) on Pt and Ta. Current-induced switching in these two samples is illustrated in Figs. 4(a) and 4(b), while the SOT efficiency as a function of the bias field is summarized in Figs. 4(c) and 4(d). First of all, from the current-induced switching polarity and SOT efficiency measurements, we note that the effective spin Hall angle of Bi_2Se_3 has the same sign with that of Pt but opposite with Ta, which is consistent with the previously reported results [11,12,18,23]. This also rules out the possibility that the spin-orbit coupling from the heavy element Tb plays the dominant role in the SOT switching, which will otherwise lead to the same switching polarities in all three samples. Second, the effective spin Hall angles of Pt and Ta are determined to be 0.017 ± 0.002 and -0.031 ± 0.002 with Eq. (1), several times smaller than those of Bi_2Se_3 and $(Bi,Sb)_2Te_3$ [Fig. 4(e)]. We note that overall, the measured spin Hall angles from Pt and Ta are smaller than the previously reported values (0.15 for Pt and −0.12 for Ta), where similar techniques but different ferromagnetic electrodes (CoFeB and Co) have been utilized [32]. This difference suggests that compared with conventional FM electrodes, the antiferromagnetically coupled CoTb layer is likely to have lower interfacial transparency [35] when it is in contact with spin-orbit materials. Therefore, the intrinsic effective spin Hall angle from Bi_2Se_3 and $(Bi,Sb)_2Te_3$ could be even larger than the measured value in this work.

Despite the increased charge-spin conversion efficiency in TI, it remains unclear whether the utilization of these materials will lead to energy advantages, as TI usually have much higher resistivity ρ compared with other spin-orbit metals. To answer this question, we calculate the power consumption for switching FM electrodes in unit magnetic volume, which is proportional to ρ/α_{SH}^2, as the critical current density for switching scales with the inverse of α_{SH}. As shown in Fig. 4(f), TI still stand out as the favorable material when power consumption is used as the comparison metric. For further optimization of the SOT efficiency, TI materials with more insulating bulk states will be beneficial, as the power dissipation in the bulk channels can be avoided. Finally, we note that in our current implementation of TI-induced switching, the shunting of current through the FM metal layer is significant. To fully exploit the efficiency of TI, magnetic semiconductors or insulators would be favorable. Potential candidates include rare-earth iron garnet or barium ferrite with PMA [36,37].

In summary, spin-orbit torque magnetic switching induced by the topological insulator is observed at room temperature. The effective spin Hall angle is precisely calibrated in Bi_2Se_3 and $(Bi,Sb)_2Te_3$ and compared with the heavy metals Pt and Ta. The large spin Hall angle suggests the robustness of charge-spin conversion in TI even at room temperature. Accompanied with recent SOT studies in TI, our work adds to the technical significance of the emerging field of topological spintronics and potentially points to practicable innovations in TI-based switching devices.

This research was partially supported by the National Science Foundation through the Massachusetts Institute of Technology Materials Research Science and Engineering Center DMR-1419807, and partially supported by the National Science Foundation under Grant No. 1639921, and the Nanoelectronics Research Corporation (NERC), a wholly owned subsidiary of the Semiconductor Research Corporation (SRC), through Memory, Logic, and Logic in Memory Using Three Terminal Magnetic Tunnel Junctions, an SRC-NRI Nanoelectronics Research Initiative Center under Research Task ID 2700.001. The Bi_2Se_3 and $(Bi,Sb)_2Te_3$ samples for this publication were provided by The Pennsylvania State University Two-Dimensional Crystal Consortium—Materials Innovation Platform (2DCC-MIP) which is supported by NSF cooperative agreement DMR-1539916.

Note added.—Recently, we noticed similar results of TI-based SOT switching of PMA layers at room temperature reported by another group [38].

*luqiao@mit.edu

[1] A. Soumyanarayanan, N. Reyren, A. Fert, and C. Panagopoulos, Nature (London) **539**, 509 (2016).
[2] V. E. Demidov, S. Urazhdin, H. Ulrichs, V. Tiberkevich, A. Slavin, D. Baither, G. Schmitz, and S. O. Demokritov, Nat. Mater. **11**, 1028 (2012).
[3] S. Emori, U. Bauer, S. M. Ahn, E. Martinez, and G. S. D. Beach, Nat. Mater. **12**, 611 (2013).
[4] W. Jiang, P. Upadhyaya, P. W. Zhang, G. Yu, M. B. Jungfleisch, F. Y. Fradin, J. E. Pearson, Y. Tserkovnyak, K. L. Wang, O. Heinonen, S. G. te Velthuis, and A. Hoffmann, Science **349**, 283 (2015).
[5] I. M. Miron, K. Garello, G. Gaudin, P.-J. Zermatten, M. V. Costache, S. Auffret, S. Bandiera, B. Rodmacq, A. Schuhl, and P. Gambardella, Nature (London) **476**, 189 (2011).
[6] L. Liu, C.-F. Pai, Y. Li, H. W. Tseng, D. C. Ralph, and R. A. Buhrman, Science **336**, 555 (2012).
[7] S. Fukami, T. Anekawa, C. Zhang, and H. Ohno, Nat. Nanotechnol. **11**, 621 (2016).
[8] M. Z. Hasan and C. L. Kane, Rev. Mod. Phys. **82**, 3045 (2010).
[9] X.-L. Qi and S.-C. Zhang, Rev. Mod. Phys. **83**, 1057 (2011).

[10] C. H. Li, O. M. J. van't Erve, J. T. Robinson, Y. Liu, L. Li, and B. T. Jonker, Nat. Nanotechnol. **9**, 218 (2014).
[11] K. Kondou, R. Yoshimi, A. Tsukazaki, Y. Fukuma, J. Matsuno, K. S. Takahashi, M. Kawasaki, Y. Tokura, and Y. Otani, Nat. Phys. **12**, 1027 (2016).
[12] A. R. Mellnik, J. S. Lee, A. Richardella, J. L. Grab, P. J. Mintun, M. H. Fischer, A. Vaezi, A. Manchon, E.-A. Kim, N. Samarth, and D. C. Ralph, Nature (London) **511**, 449 (2014).
[13] Y. Fan, P. Upadhyaya, X. Kou, M. Lang, S. Takei, Z. Wang, J. Tang, L. He, L.-T. Chang, M. Montazeri, G. Yu, W. Jiang, T. Nie, R. N. Schwartz, Y. Tserkovnyak, and K. L. Wang, Nat. Mater. **13**, 699 (2014).
[14] Y. Fan, X. Kou, P. Upadhyaya, Q. Shao, L. Pan, M. Lang, X. Che, J. Tang, M. Montazeri, K. Murata, L.-T. Chang, M. Akyol, G. Yu, T. Nie, K. L. Wong, J. Liu, Y. Wang, Y. Tserkovnyak, and K. L. Wang, Nat. Nanotechnol. **11**, 352 (2016).
[15] K. Yasuda, A. Tsukazaki, R. Yoshimi, K. Kondou, K. S. Takahashi, Y. Otani, M. Kawasaki, and Y. Tokura, arXiv:1612.06862.
[16] Y. Shiomi, K. Nomura, Y. Kajiwara, K. Eto, M. Novak, K. Segawa, Y. Ando, and E. Saitoh, Phys. Rev. Lett. **113**, 196601 (2014).
[17] H. Wang, J. Kally, J. S. Lee, T. Liu, H. Chang, D. R. Hickey, K. A. Mkhoyan, M. Wu, A. Richardella, and N. Samarth, Phys. Rev. Lett. **117**, 076601 (2016).
[18] M. Jamali, J. S. Lee, J. S. Jeong, F. Mahfouzi, Y. Lv, Z. Zhao, B. K. Nikolic, K. A. Mkhoyan, N. Samarth, and J.-P. Wang, Nano Lett. **15**, 7126 (2015).
[19] Y. Wang, P. Deorani, K. Banerjee, N. Koirala, M. Brahlek, S. Oh, and H. Yang, Phys. Rev. Lett. **114**, 257202 (2015).
[20] J. Tang, L.-T. Chang, X. Kou, K. Murata, E. S. Choi, M. Lang, Y. Fan, Y. Jiang, M. Montazeri, W. Jiang, Y. Wang, L. He, and K. L. Wang, Nano Lett. **14**, 5423 (2014).
[21] Y. Ando, T. Hamasaki, T. Kurokawa, K. Ichiba, F. Yang, M. Novak, S. Sasaki, K. Segawa, Y. Ando, and M. Shiraishi, Nano Lett. **14**, 6226 (2014).
[22] A. Dankert, J. Geurs, M. Kamalakar, S. Charpentier, and S. Dash, Nano Lett. **15**, 7976 (2015).
[23] L. Liu, A. Richardella, I. Garate, Y. Zhu, N. Samarth, and C.-T. Chen, Phys. Rev. B **91**, 235437 (2015).
[24] Z. Jiang, C. Z. Chang, M. R. Masir, C. Tang, Y. Xu, J. S. Moodera, A. H. MacDonald, and J. Shi, Nat. Commun. **7**, 11458 (2016).
[25] P. Hansen, C. Clausen, G. Much, M. Rosenkranz, and K. Witter, J. Appl. Phys. **66**, 756 (1989).
[26] J. Finley and L. Liu, Phys. Rev. Applied **6**, 054001 (2016).
[27] A. Richardella, D. M. Zhang, J. S. Lee, A. Koser, D. W. Rench, A. L. Yeats, B. B. Buckley, D. D. Awschalom, and N. Samarth, Appl. Phys. Lett. **97**, 262104 (2010).
[28] See Supplemental Material at http://link.aps.org/supplemental/10.1103/PhysRevLett.119.077702 for sample characterization using x-ray diffraction and atomic force microscopy, anomalous Hall resistance with an in-plane bias field, estimation of the Dzyaloshinskii-Moriya interaction energy, and magnetization in $(\mathrm{Bi,Sb})\mathrm{Te}_3/\mathrm{CoTb}$, Pt/CoTb, and Ta/CoTb samples, which includes references [26,29–31].
[29] J. J. Turner, X. Huang, O. Krupin, K. A. Seu, D. Parks, S. Kevan, E. Lima, K. Kisslinger, I. McNulty, R. Gambino, S. Mangin, S. Roy, and P. Fischer, Phys. Rev. Lett. **107**, 033904 (2011).
[30] Y. Tserkovnyak and D. Loss, Phys. Rev. Lett. **108**, 187201 (2012).
[31] K. Nomura and N. Nagaosa, Phys. Rev. B **82**, 161401 (2010).
[32] C.-F. Pai, M. Mann, A. J. Tan, and G. S. D. Beach, Phys. Rev. B **93**, 144409 (2016).
[33] Y. Zhang, K. He, C.-Z. Chang, C.-L. Song, L.-L. Wang, X. Chen, J.-F. Jia, Z. Fang, X. Dai, W.-Y. Shan, S.-Q. Shen, Q. Niu, X.-L. Qi, S.-C. Zhang, X.-C. Ma, and Q.-K. Xue, Nat. Phys. **6**, 584 (2010).
[34] J. Zhang, C. Z. Chang, Z Zhang, J. Wen, X. Feng, K. Li, M. Liu, K. He, L. Wang, X Chen, Q.-K. Xue, X. Ma, and Y. Wang, Nat. Commun. **2**, 574 (2011).
[35] W. Zhang, W. Han, X. Jiang, S. H. Yang, and S. S. P. Parkin, Nat. Phys. **11**, 496 (2015).
[36] C. O. Avci, A. Quindeau, C.-F. Pai, M. Mann, L. Caretta, A. S. Tang, M. C. Onbasli, C. A. Ross, and G. S. D. Beach, Nat. Mater. **16**, 309 (2017).
[37] P. Li, T. Liu, H. C. Chang, A. Kalitsov, W. Zhang, G. Csaba, W. Li, D. Richardson, A. DeMann, G. Rimal, H. Dey, J. Jiang, W. Porod, S. B. Field, J. K. Tang, M. C. Marconi, A. Hoffmann, O. Mryasov, and M. Z. Wu, Nat. Commun. **7**, 12688 (2016).
[38] M. DC, M. Jamali, J.-Y. Chen, D. R. Hickey, D. Zhang, Z. Zhao, H. Li, P. Quarterman, Y. Lv, M. Li, K. A. Mkhoyan, and J.-P. Wang, arXiv:1703.03822.